Enthalpy/Entropy Compensation Effects from Cavity Desolvation Underpin Broad Ligand Binding Selectivity for Rat Odorant Binding Protein 3

ARTICLE *in* BIOCHEMISTRY · MARCH 2014

Impact Factor: 3.02 · DOI: 10.1021/bi5002344 · Source: PubMed

7 AUTHORS, INCLUDING:

Stephen B Carr
Research Complex at Harwell
22 PUBLICATIONS **356** CITATIONS
SEE PROFILE

Loic Briand
Center for Taste and Feeding Behaviour
85 PUBLICATIONS **1,388** CITATIONS
SEE PROFILE

David Jan Scott
University of Nottingham
90 PUBLICATIONS **1,587** CITATIONS
SEE PROFILE

BIOCHEMISTRY
including biophysical chemistry & molecular biology

Article

pubs.acs.org/biochemistry

Enthalpy/Entropy Compensation Effects from Cavity Desolvation Underpin Broad Ligand Binding Selectivity for Rat Odorant Binding Protein 3

Katherine L. Portman,[†,‡] Jed Long,[‡] Stephen Carr,[§] Loïc Briand,[#] Donald J. Winzor,[⊥] Mark S. Searle,*[,‡] and David J. Scott*[,†,§]

[†]National Centre for Macromolecular Hydrodynamics, School of Biosciences, University of Nottingham, Sutton Bonington LE12 5RD, United Kingdom

[‡]School of Chemistry, Centre for Biomolecular Sciences, University of Nottingham, Nottingham NG7 2RD, United Kingdom

[§]ISIS Neutron and Muon Source and Research Complex at Harwell, Rutherford Appleton Laboratory, Oxfordshire OX11 0FA, United Kingdom

[#]Centre des Sciences du Goût et de l'Alimentation, INRA UMR1324, CNRS UMR6265, Université de Bourgogne, F-21000 Dijon, France

[⊥]School of Chemistry and Molecular Biosciences, University of Queensland, Queensland 4072, Australia

ABSTRACT: Evolution has produced proteins with exquisite ligand binding specificity, and manipulating this effect has been the basis for much of modern rational drug design. However, there are general classes of proteins with broader ligand selectivity linked to function, the origin of which is poorly understood. The odorant binding proteins (OBPs) sequester volatile molecules for transportation to the olfactory receptors. Rat OBP3, which we characterize by X-ray crystallography and NMR, binds a homologous series of aliphatic γ-lactones within its aromatic-rich hydrophobic pocket with remarkably little variation in affinity but extensive enthalpy/entropy compensation effects. We show that the binding energetics are modulated by two desolvation processes with quite different thermodynamic signatures. Ligand desolvation follows the classical hydrophobic effect; however, cavity desolvation is consistent with the liberation of "high energy" water molecules back into bulk solvent with a strong, but compensated, enthalpic contribution, which together underpin the origins of broad ligand binding selectivity.

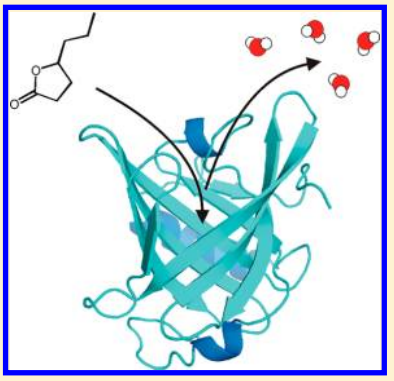

The biological function of many protein structures has been honed through evolution to bind with exquisite specificity to one particular ligand. Understanding and manipulating this effect has underpinned much of modern drug design. However, there are general classes of proteins those functional role is based upon much broader ligand binding selectivity,[1,2] the molecular origins of which are far less well understood. An underlying factor is the phenomenon of enthalpy/entropy (H/S) compensation which is widely reported in both biomolecular and supramolecular host−guest recognition studies.[3−8] A general description of the origins of this phenomenon similarly remains elusive and controversial,[9−14] not least because of the experimental difficulties of disaggregating the relative contributions to binding and in particular the role that the solvent plays in this process.[15−19]

It is well-recognized that reorganization of the solvent structure associated with a ligand and protein cavity, both free and in the bound state, is an important mechanistic factor in driving ligand binding and in understanding classic hydrophobic interactions.[20,21] However, models for protein cavity solvent structure and energetics are inherently poorly defined and reliant on simulation studies. In addition, protein structures have proved particularly challenging to enthalpy/entropy compensation analysis because of the uncertainties over the relative entropic contributions from changes in ligand and protein dynamics which are balanced against tighter local contacts or global (enthalpic) changes in structure and bonding.[22,23]

Odorant binding proteins (OBPs), which are small (17−20 kDa) proteins found in the nasal mucous that coats the olfactory epithelium,[24] possess the property of binding to a broad range of hydrophobic volatile odorant molecules with low micromolar affinity[25−28] and facilitate transportation to the olfactory receptors.[29] This role is typical of the lipocalin protein family which encompasses a range of small antiparallel β-barrel proteins that transport or store a range of low-solubility or chemically sensitive biomolecules.[1,2] The underlying structural and thermodynamic principles by which OBPs achieve broad ligand selectivity is of particular interest.

We have focused our studies on rat OBP3, one of three subtypes with <30% sequence homology, which binds simple aliphatic heterocycles.[30−34] We have employed X-ray crystallog-

Received: February 24, 2014
Revised: March 21, 2014
Published: March 26, 2014

dx.doi.org/10.1021/bi5002344 | *Biochemistry* 2014, 53, 2371−2379

raphy to define the structure of rat OBP3 and NMR spectroscopy to probe ligand-induced changes in structure and dynamics as molecules are accommodated in the highly nonpolar aromatic-rich cavity. Isothermal titration calorimetry (ITC) analysis reveals striking insights into the thermodynamics of binding of a homologous series of aliphatic γ-lactones to both *wt*-OBP3 and a number of Phe → Ala OBP3 cavity mutants. Despite the observation of relatively little variation in binding free energy either within the family of γ-lactones or between *wt*-OBP3 and the mutants, we observe large compensating variations in the enthalpy and entropy of interaction. The analysis suggests that the binding energetics are modulated by two distinct desolvation processes corresponding to (i) the classical hydrophobic interaction model involving release to bulk solvent of highly ordered water molecules from the nonpolar ligand surface (ΔS positive, ΔH positive), and (ii) desolvation of the protein binding cavity by liberating "high energy" water back into solution (ΔS negative, ΔH negative).

Although both of the processes described represent a "hydrophobic interaction", arising from desolvation of a nonpolar environment, it is striking that these two phenomena are associated with contrastingly different thermodynamic signatures. Only one of these has the favorable entropic characteristics of the classical hydrophobic effect.[20,21] However, reports that reorganization of weakly bound disordered water from apposing surfaces provides a significant portion of the binding enthalpy are consistent with this model.[35−37] The physical insights into the nature and energetics of the networks of solute-associated water molecules, which either remain bound,[14] or are expelled into bulk solvent by the ligand binding event,[35] strengthen the arguments that, alongside the evolution of the architecture of the protein binding cavity, water molecules play a critical role in driving the thermodynamics of ligand binding and in understanding both H/S compensation phenomenon and the origins of broad ligand binding selectivity.

MATERIALS AND METHODS

Protein Expression, Purification, and Crystallization. Recombinant rat OBP3 was expressed as a His-tagged protein to allow its purification by affinity chromatography on nickel-chelating Sepharose,[31] after which it was further purified by size-exclusion chromatography on a Superdex 75 column (1.0 × 75 cm). Any ligands present in the OBP3 binding pocket were then removed by ethanol precipitation of the protein[38] before lyophilization to remove any remaining ethanol. Mass spectrometry (ESI-TOF) of the purified material yielded a molecular mass of 19 897 Da, which matches the value calculated from the sequence of the recombinant rat OBP3.

Structure Determination and Refinement. OBP3 was crystallized in 0.02 M D-glucose, 0.02 M D-galactose, 0.02 M L-fucose, 0.02 M D-xylose, 0.02 M *N*-acetyl-D-glucosamine, 0.1 M morpheus buffer 1 pH 6.5, 10% w/v polyethylene glycol 20000, 20% polyethylene glycol 550. Thin platelike crystals took approximately 1 month to grow to 75 μm in size. They were then flash-cooled in liquid N_2 prior to data collection. X-ray diffraction data were collected on beamline I24 (Diamond Light Source, UK) and reduced using MOSFLM[39] and SCALA.[40] Initial phase estimates were obtained by molecular replacement using MRBump,[41,42] and the resulting electron density maps were inspected in COOT.[43] Iterative rounds of manual rebuilding and refinement using REFMAC[44] were used to complete the model which contained four protein molecules in the asymmetric unit. B-factors (main chain and side chains in Å^2) were determined for each of the four chains (A−D) (Chain A, 42.0 and 46.5; Chain B, 39.9 and 44.2; Chain C, 44.5 and 48.7; Chain D, 41.9 and 46.9). Structure validation was performed using the Molprobity web server[45] throughout the modelling and refinement process.

Determination of Thermodynamic Parameters by ITC. Commercial preparations (from Sigma-Aldrich) of the γ-lactones (liquids) were diluted with phosphate-buffered saline (1.75 mM KH_2PO_4, 10 mM Na_2HPO_4, 137 mM NaCl, 2.7 mM KCl), pH 7.4, to obtain 300 μM solutions of each. For ITC experiments, conducted at 25 °C in a Microcal VP-Auto ITC apparatus (GE Healthcare), 30 μM OBP3 in the same phosphate-buffered saline was titrated with successive 14 μL aliquots of the above ligand stock solutions to generate binding curves that were subjected to standard analysis[46] to obtain ΔH^0, the dissociation constant (K_d), $T\Delta S^0$, and ΔG^0. Experiments were performed in triplicate, and errors reflect the standard deviation from the mean value.

NMR Studies. Doubly labeled ($^{15}N/^{13}C$) OBP3 was prepared in standard minimal media supplemented with $^{15}NH_4Cl$ and uniformly labeled ^{13}C-glucose. A Bruker-600 MHz spectrometer has been used to obtain all NMR spectra, which were acquired by standard procedures at 298 K. Briefly, solutions (1 mM) of $^{15}N/^{13}C$ labeled OBP3 were prepared in potassium phosphate buffered buffer pH 7.0. Backbone assignments were carried out using triple resonance experiments HNCO, HN(CA)CO, CBCANH, and CBCA(CO)NH.[47−50] Assignments of specific residues were greatly aided by use of "unlabelling" experiments,[51,52] where various amino acids (Lys, Arg, Thr, and Gln) were systematically supplemented during protein expression.

RESULTS

Structure of Rat OBP3. In the absence of a structure for rat OBP3, we crystallized a recombinant form of the protein which yielded diffraction data to 2.8 Å resolution (Table 1). There are four molecules (chains A−D) in the asymmetric unit, reflecting crystal packing interactions, since size exclusion chromatography shows OBP3 to be monomeric in solution. The overall structure is typical of a lipocalin fold in that it comprises the characteristic seven-stranded β-sheet with a single α-helix capping the central binding cavity (Figure 1A). Overall, with the exception of the N-terminus, the structure is relatively rigid as evidenced by the low B-factors (30−40 Å^2) observed for the β-sheet residues forming the pocket. The single α-helix exhibits a slightly higher set of B-factors than the rest of the protein (45−60 Å^2), indicating that it is potentially more flexible and consistent with a flexible hinge that allows ligand access to the cavity.

OBP3 has a larger pocket size (466 Å^3) than previously seen in OBP1 (326−328 Å^3),[53] which confers on OBP3 the potential to sequester larger ligands. The pocket is largely hydrophobic and lined with aromatic residues, whose side chains are well defined by the electron density (Figure 1B). The cavity is capped by a single tyrosine (Y103) which occludes the pocket from the bulk solvent (Figure 1C) in the manner observed for OBP1 and the mouse major urinary proteins (MUPs).[54,55] Although OBP3 was crystallized from ligand-free preparations, we observed density in the pocket, a feature also observed in our structure of OBP1,[53] which is most likely associated with small sugars or cosolute molecules captured

dx.doi.org/10.1021/bi5002344 | *Biochemistry* 2014, 53, 2371−2379

Table 1. X-ray Data Collection and Refinement Statistics for Rat OBP3[a]

space group	$P2_1$
cell dimensions (Å)	a = 62.98, b = 100.53, c = 72.41, β = 110.61
resolution (Å)	67.9–2.80 (2.95–2.80)
completeness	95.7 (95.1)
multiplicity	1.8 (1.8)
$\langle I/\sigma \rangle$	4.8 (1.9)
R_{merge}[b]	13.1 (47.5)
R_{pim}[c]	11.9 (42.7)
Refinement	
R_{work}/R_{free}[d]	21.8/24.9
Model	
protein atoms	5024
RMSD from ideal	
bond lengths (Å)	0.011
bond angles (°)	1.372
Ramachandran favored (%)	97.6
Ramachandran outliers (%)	0

[a]Values in parentheses refer to data in the highest resolution shell. [b]$R_{merge} = \Sigma_{hkl}\Sigma_i|I_i(hkl) - \langle I_i(hkl)\rangle|/\Sigma_{hkl}\Sigma I_i(hkl)$, where $I_i(hkl)$ is the intensity of reflection hkl, $\langle I_i(hkl)\rangle$ is the mean intensity of multiple corresponding symmetry related reflections, and Σ_i is the sum over all i measurements of reflection hkl. [c]$R_{pim} = \Sigma_{hkl}[1/(N-1)]^{1/2}\Sigma_i|I_i(hkl) - \langle I_i(hkl)\rangle|/\Sigma_{hkl}\Sigma I_i(hkl)$, where $I_i(hkl)$, $\langle I_i(hkl)\rangle$, Σ_i are as defined for R_{merge} and N is the multiplicity of a given reflection.. [d]$R_{work} = \Sigma_{hkl}||F_{obs}| - |F_{calc}||/\Sigma_{hkl}|F_{obs}|$ where F_{obs} and F_{calc} are the observed and calculated structure factors respectively. R_{free} is calculated in the same manner but using a random subset (5%) of reflections that are excluded from refinement.

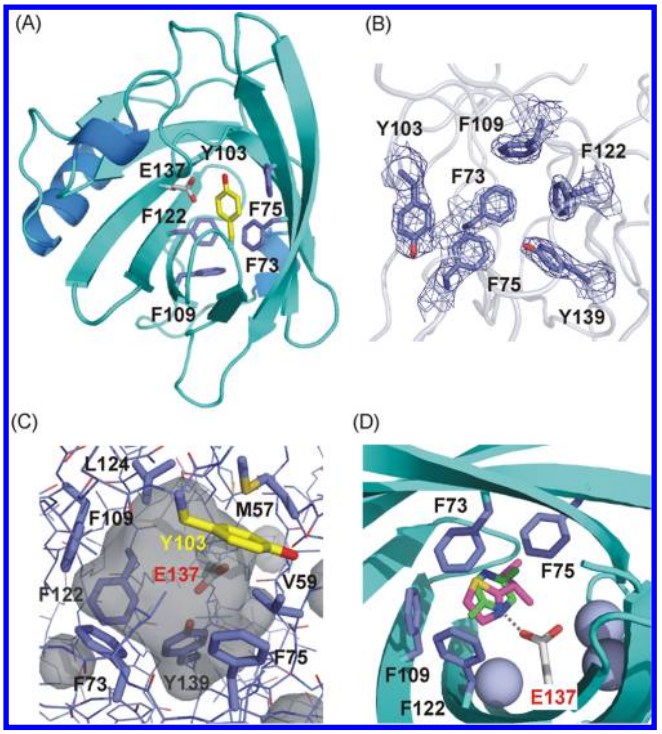

Figure 1. (A) Crystal structure of rat OBP3 showing the seven-stranded β-barrel fold and α-helix that are characteristic features of the lipocalin protein family. The largely hydrophobic and aromatic binding pocket is capped by Y103 (yellow) but contains a polar residue E137. Aromatic residues that have been mutated to Ala are highlighted. (B) Electron density map for several of the aromatic side chains involved in ligand binding (density shown is $2F_o-F_c$ map contoured at 1.2σ). (C) Illustration of the >400 Å^3 ligand-accessible pocket (shaded region) with key hydrophobic residues highlighted, together with the polar residue E137 at the base of the cavity. (D) Homology model using X-ray coordinates of OBP3 overlaid with MUP IV complexes showing the likely position of bound pyrazine (light blue; PDB code 3kfi) and thiazole ligands (green; PDB code 3kff) (ligands **2** and **3** in Figure 2) which form a single-point H-bond contact to E118 in MUP IV. Bound water molecules in the MUP IV complexes, which solvate the E118 side chain and bridge with main chain hydrogen bond donors and acceptors, are shown as spheres. This residue is conserved as E137 in OBP3 (as shown).

from the crystallization liquor. We were unable to assign unambiguously a single ligand type to this density, consistent with some heterogeneity of bound molecules in the cavity.

The binding pockets of the OBPs contain few polar residues; however, E137 is found in a prominent position within the cavity of OBP3 and, by homology with MUP IV (which has the same conserved residue, E118), is likely to play a central role in anchoring ligands within the cavity. A number of MUP IV ligand-bound structures have been determined that show a single-point hydrogen bond from the protonated E118 to alcohol, ketone, pyrazine, and thiazole ligands. In all complexes of MUP IV, two or three water molecules are closely associated with the E118 side chain presumably to partially offset the energetic cost of burying the polar side chain within an otherwise hydrophobic cavity. Homology models with OBP3 (Figure 1D) suggest that bound ligands can be accommodated in a similar manner via contact with E137. In contrast, OBP1 shows some subtle differences to OBP3: E137 is substituted for L137, but OBP1 compensates by introducing a hydrogen bond donor/acceptor in the form of L124N substitution at an adjacent position.

Thermodynamics of γ-Lactone Binding. The work of Löbel et al.[31,32] has shown that a wide variety of simple aliphatic esters, ketones, substituted aromatics, and small heterocycles bind with similar affinities to OBP3. Our own ITC measurements on a subset of odorants show equilibrium binding affinities in the range 10^5–10^7 M^{-1} (Figure 2). We have specifically focused on the thermodynamics of the homologous series of aliphatic γ-lactones. Like many other small ligand–protein interactions,[14,54,55] the γ-heptalactone (n = 2) binds in an enthalpy-driven process with a large negative entropy change (Figure 3A). The latter is consistent with the loss of translational and rotational freedom associated with the bimolecular association process and masks the anticipated entropic contributions from classical hydrophobic desolvation effects. Increasing the aliphatic chain length from γ-heptalactone (n = 2) to the undecalactone (n = 6) realizes a further ca. 130 Å^2 of ligand nonpolar surface area but, surprisingly, does not give rise to an increase in binding affinity through further burial of the longer apolar side chain (Figure 3A). Indeed, the measured standard free energy change (ΔG^0) for the interaction in phosphate-buffered saline (pH 7.4) is very similar for all five ligands, with ΔG^0 = −31.4 (±3.3) kJ mol^{-1}, where the uncertainty is expressed as twice the standard deviation of the mean. An additional entropic contribution that correlates with increasing chain length is clearly evident. However, a strong H/S compensation (Figure 3B) completely negates the entropic advantage (at 25 °C), with a variation in ΔH^0 across the series of −70 to −30 kJ mol^{-1}. More formally,

dx.doi.org/10.1021/bi5002344 | Biochemistry 2014, 53, 2371–2379

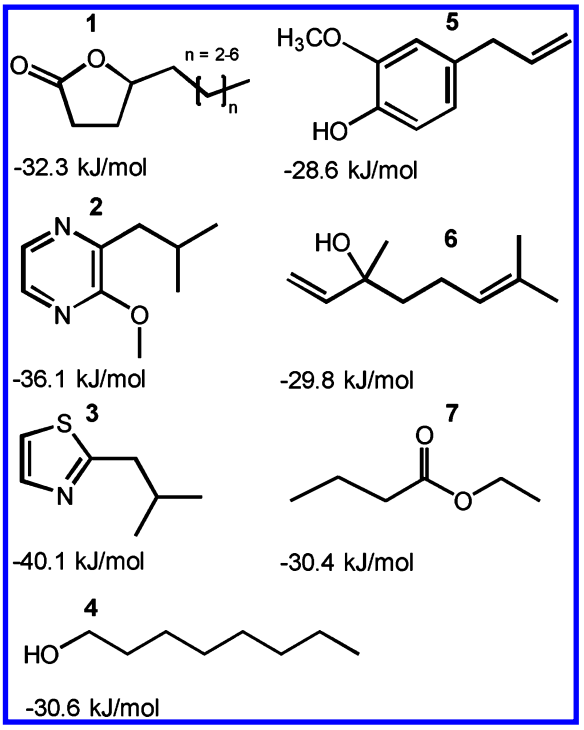

Figure 2. Structures of a diverse collection of odorant molecules characterized by ITC with OBP3. Binding free energies determined at 298 K are shown.

rearranging the Gibbs–Helmholtz equation to $\Delta H^0 = \Delta G^0 + T\Delta S^0$ and plotting ΔH^0 against $T\Delta S^0$ (Figure 3B) gives an intercept with a value from unconstrained linear regression analysis for ΔG^0 of −31.1 (±3.0) kJ mol^{-1} and a slope of 1.02 (±0.12).

Thus, across the series we see the expected classical entropic contribution to binding with the increase in apolar surface area of the ligand[20,21] and a compensatory reduction in the enthalpy of binding consistent with the disruption of ordered solvent structure. However, although the hydrophobic interaction is regarded as providing an effective driving force for molecular recognition in aqueous solution,[56] here we observe compensatory effects that fully negate this entropic advantage and thereby suggest a more complex underlying mechanism.

What other contributions should be considered? First, entropic effects from any reductions in dynamics of the aliphatic ligands would be expected to partially offset any entropic advantage from solvent release,[13,22,23] and second, ligand–protein dispersive interactions arising from the increasing van der Waals surface area across the series of ligands would be predicted to make the interaction more exothermic, contrary to observations. Any such contributions have to be considered integral to the experimental measurements and cannot readily be disaggregated. An interpretation of the ITC results solely in terms of H/S compensatory solvation effects, of course, would be conditional upon the absence of marked changes in overall protein structure and dynamics as the result of ligand binding.[22,23]

NMR Studies of OBP3–Ligand Complexes. We examined the effects of ligand binding on OBP3 structure and dynamics by NMR, for which the almost complete backbone assignment for apo-OBP3 was obtained using two- and three-dimensional (2D and 3D) methods combined with global isotopic labeling, and selective unlabeling, strategies.[54] Ligand-induced chemical shift perturbations (CSP) for OBP3

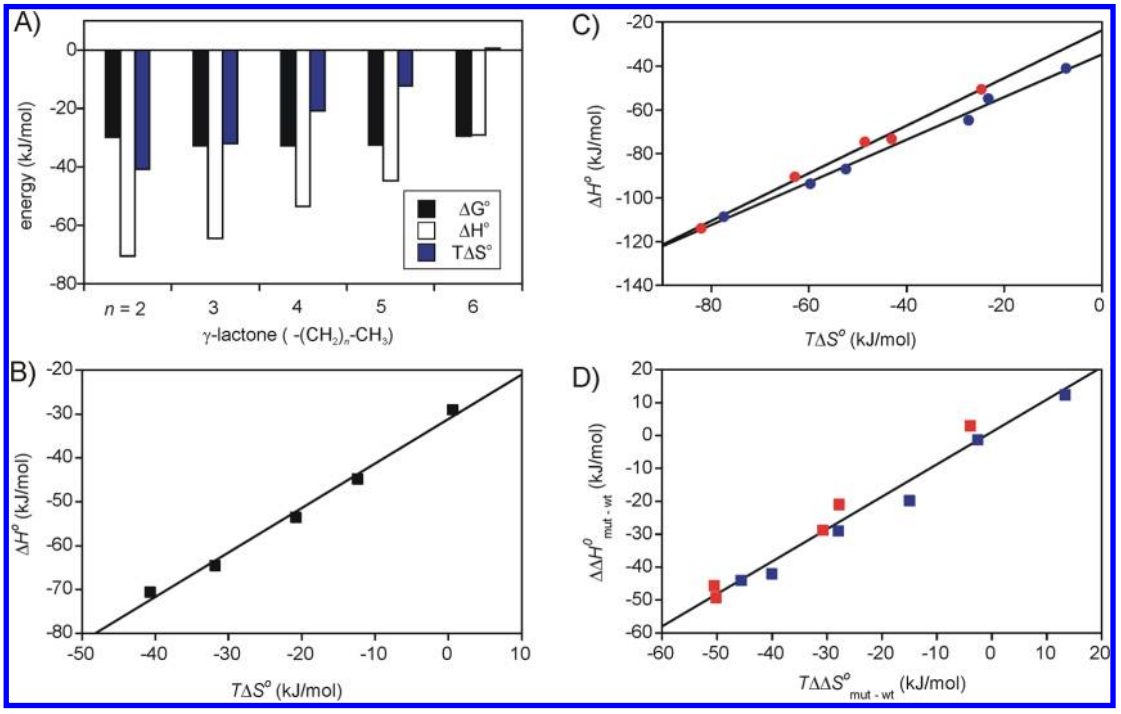

Figure 3. Experimental demonstration of the enthalpy–entropy (H/S) compensation phenomenon by an ITC investigation of the interaction between a series of γ-lactones and OBP3 in phosphate buffered saline (pH 7.4) thermostatically maintained at 25 °C. (A) Free energy, enthalpy, and entropy for binding to *wt*-OBP3; (B) H/S compensation plot for *wt*-OBP3; (C) corresponding results for F73A–F75A (blue) and F109A–F122A (red) mutant pairs; (D) difference plot (mutant − wild-type) for ligand binding to estimate contribution from solvation effects in the expanded cavity of the mutants.

dx.doi.org/10.1021/bi5002344 | *Biochemistry* 2014, 53, 2371–2379

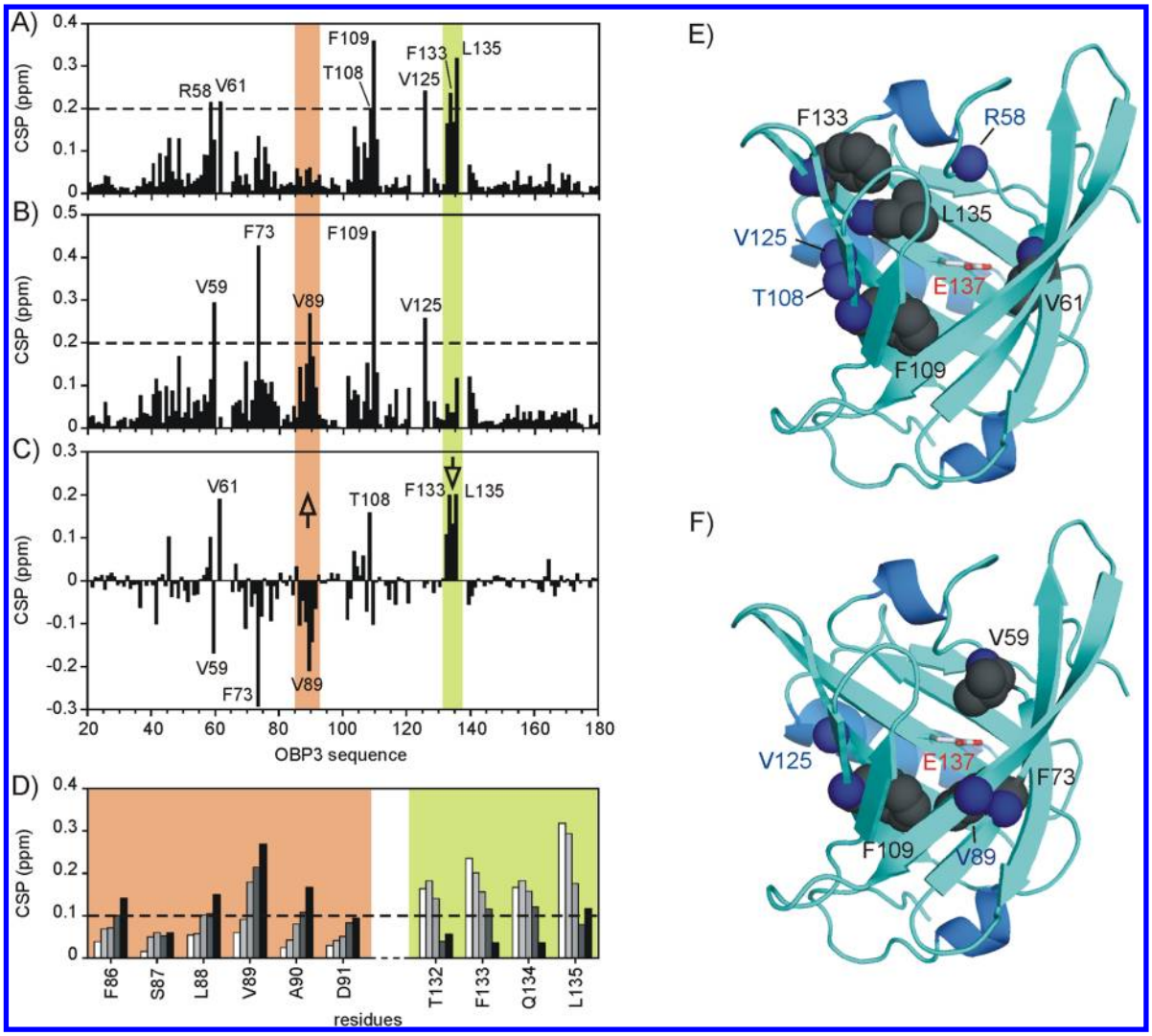

Figure 4. NMR analysis of rat OBP3 binding to γ-heptalactone (n = 2) and γ-undecalactone (n = 6). Chemical shift perturbations (CSPs) of the individual residues of rat OBP3 upon binding to (A) γ-heptalactone, (B) γ-undecalactone, and (C) difference plot. Residues with large ligand-dependent CSPs (>0.2 ppm) are labeled. (D) Highlighted CSP trends across the series of lactones for two clusters of residues that show changes in the binding locus of the ligand with chain length. Ribbon diagrams of OBP3 identifying the residues that exhibit significant chemical shift perturbations (CSP > 0.2 ppm) in TROSY NMR spectra of the apoprotein and its complexes with γ-heptalactone (E) and with γ-undecalactone (F), nitrogen atoms shown in blue and labeled. Perturbed residues whose side chains point into the binding cavity are shown with van der Waals spheres in dark gray. The side chain of E137 is shown in stick format.

were determined as a function of primary sequence for all of the γ-lactones. The data for γ-heptalactone and γ-undecalactone are shown in Figure 4A,B, together with the difference plot (C). With an average CSP over 145 assigned residues of <0.05 ppm, we conclude that ligand binding mediates no global structural rearrangements. However, many residue-specific effects between 0.1 to 0.4 ppm are indicative of significant ligand-induced perturbations. Our analysis of γ-heptalactone binding to OBP3 (Figure 4A) identified 18 residues with CSP effects > 0.1 ppm, with a subset of 7 residues showing effects > 0.2 ppm, which we analyzed further. Four of these (V61, F109, F133, and L135) are key hydrophobic β-sheet residues that point into the binding cavity (Figure 4E). F133 and L135 on strand H are adjacent to E137, which, although not assigned, is implicated as a ligand anchor point within the cavity, as shown by analogy with MUP IV in Figure 1C. A further three perturbed residues (R58, T108, and V125) are part of the same hydrogen bonded backbone network but have side chains on the outer (solvent exposed) face of the β-sheet or (in the case of R58) are in a loop connecting two strands of sheet. Those key residues with large CSPs that are found within the cavity and likely to be involved in direct ligand contacts are mapped onto the structure of OBP3 in Figure 4E.

Taking γ-heptalactone as a reference point, we also looked for differences as a function of aliphatic chain length to identify new interactions that accommodate the longer side chains. Surprisingly, we see not only residues whose CSPs increase in a ligand-dependent manner (Figure 4D) but others that decrease showing significant CSP effects for the shorter ligands but diminishing effects with the longer lactones, and vice versa. Two particular clusters of residues are highlighted. The first is the hydrophobic patch within the cavity formed by V61, F109, F133, and L135, as highlighted above, which experience the largest CSP effects of >0.2 ppm with γ-heptalactone (Figure 4A). As is evident for γ-undecalactone in Figure 4B, and in the difference plot Figure 4C, the CSP effects for these same

dx.doi.org/10.1021/bi5002344 | Biochemistry 2014, 53, 2371−2379

residues (with the exception of F109) diminish across the ligand series (Figure 4D), suggesting that the longer aliphatic ligands no longer employ the same binding patch. In contrast, a new cluster of residues emerges as key contacts, including V59, F73, and V89. Mapping these residues onto the structure (Figure 4F) identifies a new hydrophobic patch that lies deeper into the cavity. A number of residues, notably F109 and V125, which are adjacent to N107, show similar and significant perturbations in all of the complexes studied. These unexpected ligand-dependent and residue-specific differences suggest some structural adaptability of the highly aromatic pocket in accommodating hydrophobic ligands of different sizes in potentially different orientations.

A further consideration is that the entropic contributions to ligand binding affinity in part reflects changes in protein dynamics which we can assess through backbone ^{1}H-^{15}N heteronuclear NOE measurements. An average NOE value of 0.76 for the apoprotein indicates a fairly rigid overall structure with some smaller values, typically in the loop regions, suggesting local backbone flexibility. The NOE data for five OBP3 ligand complexes (0.77 ± 0.2) yielded similar average values across >140 residues suggesting little ligand-induced change in overall backbone dynamics.

Changing the Solvation of the Binding Pocket through Protein Engineering. How the architecture of the binding pocket influences solvent structure and the energetics of ligand binding was investigated by expanding the cavity by mutating a number of bulky aromatic residues (F73, F75, F109, F122; Figure 1A) to Ala and measuring the thermodynamics of γ-lactone binding by ITC. The F73A and F75A mutations showed little effect on ligand binding affinity, despite both residues displaying significant CSPs in complexes of *wt*-OBP3. In contrast, F109A and F122A mutants showed a small decrease in affinity, despite the fact that only F109 showed any significant CSP effects in the *wt*-OBP3. Despite the modest effects of the mutations on the binding affinities of the γ-lactones ($\Delta\Delta G^0$ = 0−6 kJ mol^{-1}), we observe binding to be considerably more exothermic (range −40 to −115 kJ mol^{-1}) compared to *wt*-OBP3, with strong H/S compensation effects (Figure 3C).

To separate the contributions to binding energies from ligand and cavity desolvation effects, we calculated differences in enthalpy and entropy changes ($\Delta\Delta H^0$ and $T\Delta\Delta S^0$) for a given ligand binding to *wt*-OBP3 versus different mutant OBP3s (Figure 3D). The ligand desolvation term is eliminated if assumed to be similar for each binding event, allowing us to isolate the protein desolvation effect. We see large differences and strong H/S compensation effects, which suggest that the thermodynamic signature for ligand binding is strongly influenced by the desolvation of the binding cavity. This suggested combination of hydrophobic protein−ligand interaction and protein cavity desolvation finds precedent in observations of partial solvent occupancy and dynamic disorder in X-ray structures, which led to speculation that weakly bound disordered water is likely to contribute favorably to the enthalpy of binding when displaced back into bulk solvent.[14,35] The expected thermodynamic signature for this model of stronger hydrogen bonding (favorable enthalpy) and more ordered structure (unfavorable entropy) in the bulk solvent appears to explain well the strong H/S compensation effects manifested in the difference plots derived from the mutant data in Figure 3D.

Residue Y103 was also mutated to Ala to examine the effect upon ligand binding of removing the cap from the hydrophobic pocket. ITC analysis of the Y103A mutant signified that ligand association was effectively abolished. In contrast, a more conservative Y103F substitution had only a minor effect on affinity, indicating no critical role for the Y103 hydroxyl group in binding γ-lactones, but suggesting a key role for the hydrophobic cap in modulating cavity solvation and ligand access. Molecular dynamics simulations with the related lipocalin MUP-1 drew similar conclusions[54] and further suggested that cavity solvation may be dependent on a few critical residues rather than simply the volume of available space.

DISCUSSION

We have used structural and thermodynamic studies to probe the underlying basis for broad selectivity in the binding of odorant molecules to rat OBP3. In particular, we have focused on a homologous series of γ-lactones with increasing hydrophobicity. NMR chemical shift mapping and measurement of $^{1}H-^{15}N$ heteronuclear NOEs suggest that ligand-induced perturbations are largely confined to the binding cavity rather than reflecting global changes in OBP3 structure and dynamics. However, we see from NMR CSP measurements across the series of lactones that different groups of hydrophobic residues are used to interact with different aliphatic chain lengths, consistent with gradual changes in the manner in which the cavity flexibly accommodates different ligands as the bulk of the side chain increases (Figure 4D). Thus, broad ligand binding selectivity for OBP3, in this context at least, appears in part to be mediated by the architecture of the aromatic-rich pocket and the nonspecific nature of the hydrophobic contacts made with different ligands.

Ligand Desolvation Produces the Signature of a Classic Hydrophobic Interaction. The observation of a strong underlying enthalpy-driven interaction of the γ-heptalactone, which is typical of many small molecule−protein interactions,[14,38,54,57,58] at first appears to be consistent with ligand−protein dispersion interactions between the lactone ester and the aromatic-rich cavity, and electrostatic interactions with the polar side chain E137. Despite the largely hydrophobic nature of the ligand, any favorable enthalpy of binding is overwhelmingly dominated by the adverse entropy of the bimolecular association of γ-heptalactone. However, the classic signature of the hydrophobic interaction ($T\Delta S^0$ positive, but ΔH^0 positive) becomes apparent as the energetics of the interaction are analyzed against increasing chain length, such that the γ-undecalactone has an entropy of association close to zero and the smallest enthalpy of interaction of the series (−29 kJ mol^{-1}) (Figure 3A). The linear correlation between enthalpy/entropy and increase in ligand nonpolar surface area points to this as a manifestation of ligand desolvation. However, binding does not become increasingly "entropy-driven" because we see complete H/S compensation, which negates any enhancement in binding free energy, an effect that is also implicit in the Kauzman[20] treatment of the hydrophobic interaction but is frequently overlooked in published studies that have questioned the credibility of enthalpy−entropy compensation effects.[9−11]

Cavity Desolvation Contributes to the Enthalpy of Ligand Binding. We probed OBP3 cavity solvation effects further by using the protein engineering approach (Phe → Ala) to increase the cavity volume. Surprisingly, we see a further

dx.doi.org/10.1021/bi5002344 | *Biochemistry* 2014, 53, 2371−2379

significant enthalpic contribution to complex formation. The γ-octalactone, as a particular example, binds with an enthalpy of interaction with *wt*-OBP3 of −64.5 kJ mol^{-1} but to the various Phe mutants with ΔH^0 in the range −93.5 to −113.8 kJ mol^{-1}. The same trend is clearly evident across the lactone family (Figure 3C).

We considered several possible scenarios. Increases in enthalpy on the basis of changes in van der Waals/dispersive interactions between protein and ligand are anticipated to be ligand surface area dependent and, for a given ligand, either similar or even diminished by the increase in cavity volume through the reduction in protein−ligand contacts. Alternatively, the expanded binding cavity of the mutants has the potential to the accommodate a larger number of solvent molecules. A higher occupancy of "high energy" waters captured within the cavity then provides a stronger enthalpy of ligand binding when the solvent is displaced into bulk solution. This hypothesis is consistent with previous models of enthalpic contributions from the displacement of weakly ordered solvent structure associated with partial site occupancy.[35,57,58] Moreover, molecular dynamics simulations of related lipocalins[54] suggest that there is low solvent density in the cavity (only a 20% solvent occupancy of available space) which reflects cavity architecture, amino acid composition, and poor solvent−solute interactions. It is striking, however, that any enthalpic benefit from the displacement of "high energy" water via this mechanism does not provide any enhancement in binding free energy because again adverse entropic effects (which we assume to be associated with the formation of the more ordered hydrogen bonded network found in bulk solvent) fully compensate.

How many water molecules would be required to account for the observed enthalpic benefits? Experimental estimates for the enthalpy of formation of a single hydrogen bond in the gas phase range from −12 to −25 kJ mol^{-1}.[54] These estimates would suggest that we can rationalize the changes in ligand binding enthalpy to OBP3 mutants on the basis of net differences in the formation of only a few new hydrogen bonds arising from transfer of perhaps only a single additional water molecule from a highly nonpolar "high energy" environment to bulk solvent. This rough analysis would also appear to be consistent with the cavity space of ca. 100 Å^3 generated by the mutation of a Phe side chain to Ala.

A contrasting water-centric analysis of significant H/S compensation effects associated with indistinguishable changes in binding affinity has been described for a series of fluorinated benzothiazole sulphonamide ligands binding to human carbonic anhydrase (HCA).[14] The conclusions, based on high resolution X-ray structures of the complexes and ITC analysis, support the hypothesis that changes to the electronic structure of the fluorinated ligands lead to differences in the structure and thermodynamic properties of water molecules associated with the bound ligand that are important contributors to the H/S compensation effects.

We considered this alternative mechanism; however, compared with the effects of ligand fluorination, small differences in ligand polarity within our series of aliphatic γ-lactones are unlikely to make a significant contribution in enthalpically stabilizing any bound water surrounding the ligand. Indeed, liquid hydrocarbon/water solubility models show that there is little enthalpic benefit from water associated with nonpolar surfaces.[56] Alternatively, water could become trapped in this cavity creating a pocket of "high energy" water close to the bound ligand. By definition, this would be an endothermic process if these are weakly bound, which is counter to the experimental observation of enhanced ligand binding exothermicity. We conclude that the results of our mutation studies are not readily rationalized by mechanisms that require accommodation of additional water molecules in the active site around these largely nonpolar aliphatic ligands.

The explanation of enthalpy−entropy compensation effects proposed by Lumry et al.[59−61] also invokes the involvement of water molecules in the overall energetics of the ligand interaction. Earlier work on the contribution of solvent reorganization to the enthalpy of ligand binding highlighted not only many examples of strongly enthalpy-driven small-molecule−protein interactions but also X-ray structural analyses accompanied by complementary computational studies, where partial water occupancy of protein surfaces is indicative of static or dynamic disorder that may contribute a significant thermodynamic driving force for binding as water molecules are displaced into bulk solvent.[35,38] The notion that an expanded OBP3 binding cavity can accommodate one or a few more "high energy" water molecules that are subsequently expelled back into solution upon ligand binding suggests an explanation for the experimental observations. Indeed, our analysis strongly reinforces the role of solvent structural changes within the binding cavity as a key modulator of ligand binding energetics through enthalpy−entropy compensation effects.[59,61]

These rather general requirements for ligand interactions with the binding pocket are in keeping with the role of OBPs as promiscuous binders that transport a range of different odorant molecules[62] rather than a single, specific ligand. In this regard, we have demonstrated from NMR analysis at the individual residue level that there is sufficient flexibility of the binding pocket to allow its expansion to accommodate larger ligands—a feature that endows OBP3 with a potential to transport an even wider range of odorants. We have shown structurally and thermodynamically how broad binding selectivity can be achieved through the architecture of the binding cavity and the subsequent reorganization and displacement of the solvent structure within it. The latter makes a major contribution to the energetics of the interaction and contributes to the strong H/S compensation effects that appear to lead to the broad ligand binding specificity observed for OBP3.

■ ASSOCIATED CONTENT

Accession Codes

Coordinates for rat OBP3 were deposited in the Protein Data Bank under accession code 3ZQ3. Structure factors are deposited under accession code r3ZQ3sf.

■ AUTHOR INFORMATION

Corresponding Authors

*(M.S.) E-mail: mark.searle@nottingham.ac.uk. Telephone: +44 0115 951 3567.

*(D.S.) E-mail: david.scott@nottingham.ac.uk. Telephone: +44 1235 567846.

Funding

This work was funded primarily through a grant from the Biotechnology and Biological Sciences Research Council (UK) Grant BB/D522870/1 awarded to D.J.S. K.L.P.'s doctoral studentship was supported by BBSRC DTA funding to D.J.S. and M.S.S. S.C. is supported by the Medical Research Council

(UK) and J.L. by a BBSRC (UK) grant to M.S.S. This work was latterly supported by an award to D.J.S. by the Science and Technology Facilities Council. D.J.W. acknowledges the support of the University of Nottingham in providing travel and accommodation for collaborative purposes.

Notes

The authors declare no competing financial interest.

■ ACKNOWLEDGMENTS

The authors also wish to thank Anil Verma of the Oxford Protein Production Factory (UK) for help with setting up the crystallization trials.

■ REFERENCES

(1) Flower, D. R., North, A. C. T., and Sansom, C. E. (2000) The lipocalin protein family: structural and sequence overview. *Biochim. Biophys. Acta 1482*, 9−24.

(2) Grzyb, J., Latowski, D., and Strazlka, K. (2006) Lipocalins - a family portrait. *J. Plant Physiol. 163*, 895−915.

(3) Eftink, M. R., Anusiem, A. C., and Biltonen, R. L. (1983) Enthalpy-entropy compensation and heat capacity changes for protein-ligand interactions: general thermodynamic models and data for the binding of nucleotides to ribonuclease A. *Biochemistry 22*, 3884−3896.

(4) Becvar, J., and Palmer, G. (1982) The binding of flavin derivatives to the riboflavin-binding protein of egg white. A kinetic and thermodynamic study. *J. Biol. Chem. 257*, 5607−5617.

(5) Searle, M. S., and Williams, D. H. (1993) On the stability of nucleic acid structures in solution: enthalpy-entropy compensations, internal rotations and reversibility. *Nucleic Acids Res. 21*, 2051−2056.

(6) Smithrud, D. B., Wyman, T. B., and Diederich, F. (1991) Enthalpically driven cyclophane-arene inclusion complexation: solvent-dependent calorimetric studies. *J. Am. Chem. Soc. 113*, 5420−5426.

(7) Linnert, W., and Jameson, R. F. (1989) The isokinetic relationship. *Chem. Soc. Rev. 18*, 477−505.

(8) Chodera, J. D., and Mobley, D. L. (2013) Entropy-enthalpy compensation: role and ramifications in biomolecular ligand recognition and design. *Ann. Rev. Biophys. 42*, 121−142.

(9) Sharp, K. (2001) Entropy-enthalpy compensation: fact or artifact? *Protein Sci. 10*, 661−667.

(10) Cornish-Bowden, A. J. (2002) Enthalpy-entropy compensation: a phantom phenomenon. *J. Biosci. 27*, 121−126.

(11) Krishnamurthy, V. M., Bohall, B. R., Semetey, V., and Whitesides, G. M. (2006) The paradoxical thermodynamic basis for the interaction of ethylene glycol, glycine, and sarcosine chains with bovine carbonic anhydrase II: an unexpected manifestation of enthalpy/entropy compensation. *J. Am. Chem. Soc. 128*, 5802−5812.

(12) Dunitz, J. D. (1995) Win some, lose some: enthalpy-entropy compensation in weak intermolecular interactions. *Chem. Biol. 2*, 709−712.

(13) Searle, M. S., Westwell, M. S., and Williams, D. H. (1995) Application of a generalised enthalpy−entropy relationship to binding co-operativity and weak associations in solution. *J. Chem. Soc., Perkin Trans. 2 2*, 141−151.

(14) Breiten, B., Lockett, M. R., Sherman, W., Fujita, S., Al-Sayah, M., Lange, H., Bowers, C. M., Heroux, A., Krilov, G., and Whitesides, G. M. (2013) Water networks contribute to enthalpy/entropy compensation in protein-ligand binding. *J. Am. Chem. Soc. 135*, 15579−15584.

(15) Biela, A., Nasief, N. N., Betz, M., Heine, A., Hangauer, D., and Klebe, G. (2013) Dissecting the hydrophobic effect on the molecular level: the role of water, enthalpy, and entropy in ligand binding to thermolysin. *Angew. Chem., Int. Ed. 52*, 1822−1828.

(16) Lockett, M. R., Lange, H., Breiten, B., Heroux, A., Sherman, W., Rappoport, D., Yau, P. O., Snyder, P. W., and Whitesides, G. M. (2013) The binding of benzoarylsulfonamide ligands to human carbonic anhydrase is insensitive to formal fluorination of the ligand. *Angew. Chem., Int. Ed. 52*, 7714−7717.

(17) Snyder, P. W., Mecinovic, J., Moustakas, D. T., Thomas, S. W., Harder, M., Mack, E. T., Lockett, M. R., Heroux, A., Sherman, W., and Whitesides, G. M. (2011) Mechanism of the hydrophobic effect in the biomolecular recognition of arylsulfonamides by carbonic anhydrase. *Proc. Nat. Acad. Sci., U. S. A. 108*, 17889−17894.

(18) Salonen, L. M., Ellermann, M., and Diederich, F. (2011) Aromatic rings in chemical and biological recognition: energetics and structures. *Angew. Chem., Int. Ed. 50*, 4808−4842.

(19) Abel, R., Salam, N. K., Shelley, J., Farid, R., Friesner, R. A., and Sherman, W. (2011) Contribution of explicit solvent effects to the binding affinity of small-molecule inhibitors in blood coagulation factor serine proteases. *ChemMedChem 6*, 1049−1066.

(20) Kauzman, W. (1959) Some factors in the interpretation of protein denaturation. *Adv. Protein Chem. 14*, 1−63.

(21) Tanford, C. (1978) The hydrophobic effect and the organization of living matter. *Science 200*, 1012−1018.

(22) Williams, D. H., O'Brien, D. P., Sandercock, A. M., and Stephens, E. (2004) Order changes within receptor systems upon ligand binding: receptor tightening/oligomerisation and the interpretation of binding parameters. *J. Mol. Biol. 340*, 373−383.

(23) Williams, D. H., Stephens, E., O'Brien, D. P., and Zhou, M. (2004) Understanding noncovalent interactions: ligand binding energy and catalytic efficiency from ligand-induced reductions in motion within receptors and enzymes. *Angew. Chem., Int. Ed. 43*, 6596−6616.

(24) Steinbrecht, R. A. (1998) Odorant-binding proteins: expression and function. *Ann. N. Y. Acad. Sci. 855*, 323−332.

(25) Redondo, C., Vouropoulou, M., Evans, J., and Findlay, J. B. C. (2008) Identification of the retinol-binding protein (RBP) interaction site and functional state of RBPs for the membrane receptor. *FASEB J. 22*, 1043−1054.

(26) Nespoulous, C., Briand, L., Delage, M. M., Tran, V., and Pernollet, J. C. (2004) Odorant binding and conformational changes of a rat odorant-binding protein. *Chem. Senses 29*, 189−198.

(27) Borysik, A. J., Briand, L., Taylor, A. J., and Scott, D. J. (2010) Rapid odorant release in mammalian odour binding proteins facilitates their temporal coupling to odorant signals. *J. Mol. Biol. 404*, 372−380.

(28) Yabuki, M., Scott, D. J., Briand, L., and Taylor, A. J. (2011) Dynamics of odorant binding to thin aqueous films of rat-OBP3. *Chem. Senses 36*, 659−671.

(29) Matarazzo, V., Zsürger, N., Guillemot, J. C., Clot-Faybesse, O., Botto, J. M., Dal Farra, C., Crowe, M., Demaille, J., Vincent, J. P., Mazella, J., and Ronin, C. (2002) Porcine odorant-binding protein selectively binds to a human olfactory receptor. *Chem. Senses 27*, 691−701.

(30) Löbel, D., Marchese, S., Krieger, J., Pelosi, P., and Breer, H. (1998) Subtypes of odorant-binding proteins–heterologous expression and ligand binding. *Eur. J. Biochem. 254*, 318−324.

(31) Löbel, D., Jacob, M., Völkner, M., and Breer, H. (2002) Odorants of different chemical classes interact with distinct odorant binding protein subtypes. *Chem. Senses 27*, 39−44.

(32) Löbel, D., Strotmann, J., Jacob, M., and Breer, H. (2001) Identification of a third rat odorant-binding protein (OBP3). *Chem. Senses 26*, 673−680.

(33) Tegoni, M., Pelosi, P., Vincent, F., Spinelli, S., Campanacci, V., Grolli, S., Ramoni, R., and Cambillau, C. (2000) Mammalian odorant binding proteins. *Biochim. Biophys. Acta 1482*, 229−240.

(34) Vincent, F., Spinelli, S., Ramoni, R., Grolli, S., Pelosi, P., Cambillau, C., and Tegoni, M. (2000) Complexes of porcine odorant binding protein with odorant molecules belonging to different chemical classes. *J. Mol. Biol. 300*, 127−139.

(35) Chervenak, M. C., and Toone, E. J. (1994) A direct measure of the contribution of solvent reorganization to the enthalpy of binding. *J. Am. Chem. Soc. 116*, 10533−10539.

(36) Lemieux, R. U. (1996) How water provides the impetus for molecular recognition in aqueous solution. *Acc. Chem. Res. 29*, 373−380.

(37) Grunwald, E., and Steel, C. (1995) Solvent reorganization and thermodynamic enthalpy-entropy compensation. *J. Am. Chem. Soc. 117*, 5687−5692.

(38) Bingham, R. J., Findlay, J. B. C., Hseih, S-Y., Kalverda, A. P., Kjellberg, A., Perazzolo, C., Phillips, S. E. V., Seshadri, K., Trinh, C. H., Turnbull, W. B., Bodenhausen, G., and Homans, S. W. (2004) Thermodynamics of binding of 2-methoxy-3-isopropylpyrazine and 2-methoxy-3-isobutylpyrazine to the major urinary protein. *J. Am. Chem. Soc. 126*, 1675−1681.
(39) Leslie, A. G. W., and Powell, H. R. (2007) Processing diffraction data with Mosflm, in *Evolving Methods for Macromolecular Crystallography* (Reed, R. J., and Sussman, J. L., Eds.) Vol. *245*, pp 41−51, Springer, Berlin.
(40) Evans, P. R. (2006) Scaling and assessment of data quality. *Acta Crystallogr. D62*, 72−82.
(41) Keegan, R. M., and Winn, M. D. (2007) Automated search-model discovery and preparation for structure solution by molecular replacement. *Acta Crystallogr. D63*, 447−457.
(42) McCoy, A. J., Grosse-Kunstleve, R. W., Adams, P. D., Winn, M. D., Storoni, L. C., and Read, R. J. (2007) Phaser crystallographic software. *J. Appl. Crystallogr. 40*, 658−674.
(43) Emsley, P., Lohkamp, B., Scott, W. G., and Cowtan, K. (2010) Features and development of Coot. *Acta Crystallogr. D66*, 486−501.
(44) Murshudov, G. N., Vagin, A. A., and Dodson, E. J. (1997) Refinement of macromolecular structures by the maximum-likelihood method. *Acta Crystallogr. D53*, 240−255.
(45) Chen, V. B., Arendell, W. B., Headd, J. J., Keedy, D. A., Immormino, R. M., Kapral, G. J., Murray, L. W., Richardson, J. S., and Richardson, D. C. (2010) MolProbity: all-atom structure validation for macromolecular crystallography. *Acta Crystallogr. D66*, 12−21.
(46) Wiseman, T., Williston, S., Brandts, J. F., and Lin, L-N. (1989) Rapid measurement of binding constants and heats of binding using a new titration calorimeter. *Anal. Biochem. 179*, 131−137.
(47) Kay, L. E., Ikura, M., Tschudin, R., and Bax, A. (1990) Three-dimensional triple-resonance NMR spectroscopy of isotopically enriched proteins. *J. Magn. Reson. 89*, 496−514.
(48) Grzesiek, S., and Bax, A. (1992) An efficient experiment for sequential backbone assignment of medium-sized isotopically enriched proteins. *J. Magn. Reson. 99*, 201−207.
(49) Muhandiram, D. R., and Kay, L. E. (1994) Gradient-Enhanced Triple-Resonance Three-Dimensional NMR Experiments with Improved Sensitivity. *J. Magn. Reson. 103*, 203−216.
(50) Clubb, R. T., Thanabal, V., and Wagner, G. (1992) A constant-time three-dimensional triple-resonance pulse scheme to correlate intraresidue $^{1}H^{N}$, ^{15}N, and $^{13}C'$ chemical shifts in ^{15}N-^{13}C-labelled proteins. *J. Magn. Reson. 97*, 213−217.
(51) Atreya, H. S., and Chary, K. V. R. (2000) Amino acid selective "unlabelling" for residue-specific NMR assignments in proteins. *Curr. Sci. 79*, 504−507.
(52) Krishnarjuna, B., Jaipuria, G., Thakur, A., D'Silva, P., and Atreya, H. S. (2011) Amino acid selective unlabeling for sequence specific resonance assignments in proteins. *J. Biomol. NMR 49*, 39−51.
(53) White, S. A., Briand, L., Scott, D. J., and Borysik, A. J. (2009) Structure of rat odorant-binding protein OBP1 at 1.6 Å resolution. *Acta Crystallogr. D65*, 403−410.
(54) Barrett, E., Bingham, R. J., Warner, D. J., Laughton, C. A., Phillips, S. E. V., and Homans, S. W. (2005) Van der Waals interactions dominate ligand-protein association in a protein binding site occluded from solvent water. *J. Am. Chem. Soc. 127*, 11827−11834.
(55) Malham, R., Johnstone, S., Bingham, R. J., Barratt, E., Phillips, S. E. V., Laughton, C. A., and Homans, S. W. (2005) Strong solute-solute dispersive interactions in a protein-ligand complex. *J. Am. Chem. Soc. 127*, 17061−17067.
(56) Baldwin, R. L. (1986) Temperature dependence of the hydrophobic interaction in protein folding. *Proc. Natl. Acad. Sci. U. S. A. 83*, 8069−8072.
(57) Saenger, W. (1987) Structure and dynamics of water surrounding biomolecules. *Annu. Rev. Biophys. Biophys. Chem. 16*, 93−114.
(58) Rupley, J. A., and Careri, G. (1991) Protein hydration and function. *Adv. Protein Chem. 41*, 37−172.
(59) Lumry, R. (1994) In *Protein-Solvent Interactions* (Gregory, R. B., Ed.) Marcel Dekker, Inc., New York.
(60) Lumry, R., and Rajender, S. (1970) Enthalpy−entropy compensation phenomena in water solutions of proteins and small molecules: A ubiquitous property of water. *Biopolymers 9*, 1125−1227.
(61) Lumry, R. (2003) Uses of enthalpy-entropy compensation in protein research. *Biophys. Chem. 105*, 545−557.
(62) Katada, S., Hirokawa, T., Oka, Y., Suwa, M., and Touhara, K. (2005) Structural Basis for a broad but selective ligand spectrum of a mouse olfactory receptor: mapping the odorant-binding site. *J. Neurosci. 25*, 1806−1815.